Behavioral/Systems/Cognitive

Neural Correlates of Reach Errors

Jörn Diedrichsen, Yasmin Hashambhoy, Tushar Rane, and Reza Shadmehr
Laboratory for Computational Motor Control, Department of Biomedical Engineering, Johns Hopkins University, Baltimore, Maryland 21205

Reach errors may be broadly classified into errors arising from unpredictable changes in target location, called target errors, and errors arising from miscalibration of internal models (e.g., when prisms alter visual feedback or a force field alters limb dynamics), called execution errors. Execution errors may be caused by miscalibration of dynamics (e.g., when a force field alters limb dynamics) or by miscalibration of kinematics (e.g., when prisms alter visual feedback). Although all types of errors lead to similar on-line corrections, we found that the motor system showed strong trial-by-trial adaptation in response to random execution errors but not in response to random target errors. We used functional magnetic resonance imaging and a compatible robot to study brain regions involved in processing each kind of error. Both kinematic and dynamic execution errors activated regions along the central and the postcentral sulci and in lobules V, VI, and VIII of the cerebellum, making these areas possible sites of plastic changes in internal models for reaching. Only activity related to kinematic errors extended into parietal area 5. These results are inconsistent with the idea that kinematics and dynamics of reaching are computed in separate neural entities. In contrast, only target errors caused increased activity in the striatum and the posterior superior parietal lobule. The cerebellum and motor cortex were as strongly activated as with execution errors. These findings indicate a neural and behavioral dissociation between errors that lead to switching of behavioral goals and errors that lead to adaptation of internal models of limb dynamics and kinematics.

Key words: **fMRI; visual rotation; target jump; target errors; execution errors; force field; internal models; motor learning**

Introduction

Unpredictable environmental perturbations, errors in movement execution, or noise in motor production can prevent us from achieving our behavioral goals. Therefore, errors signals play an important role to help the motor system smoothly correct movements (Desmurget and Grafton, 2000). Errors may arise from different sources. For example, during reaching, target errors may occur because the target moves to a new location during the reach. In this case, the error signal is attributable to a change in the behavioral goal of the task. Alternatively, execution errors may occur because the process of transforming the goal into motor commands relied on a faulty internal model, for example, when holding a novel tool. It is not known whether the brain processes target errors differently from execution errors. Both types of errors produce smooth on-line corrections with kinematics that may be indistinguishable. However, execution errors strongly affect the internal models with which movements are controlled (Shadmehr and Mussa-Ivaldi, 1994), although the same is not known for target errors. The adaptive response to execution errors appears to depend on the cerebellum (Maschke et al., 2004; Smith and Shadmehr, 2005) and the motor cortex (Li et al., 2001; Paz et al., 2003). In contrast, on-line corrections during target errors depend on the integrity of the posterior parietal cortex (Desmurget et al., 1999) and the basal ganglia (Desmurget et al., 2004).

We hypothesized that the adaptive response to target errors might be fundamentally different from the response to execution errors. Execution errors should result in adaptation of internal models and subsequently a change in motor commands, whereas target errors should not. We compared the adaptive response after movements that had very similar trajectories but suffered from either random target errors or random execution errors. Execution errors were attributable to alterations in the kinematics of the task (i.e., visual rotation) or its dynamics (i.e., force fields). In previous work on force-field perturbations, we had observed a consistent adaptive response to errors, manifest on the subsequent trial, even when perturbations were random (Donchin et al., 2003). We confirmed this for execution errors that arose from visual perturbations. In contrast, target errors caused by discrete changes in target location led to little or no adaptive response. Therefore, although both types of error produced similar patterns of on-line correction, they affected control of the subsequent reach differently.

We followed our psychophysical results with an imaging experiment. We constructed a functional magnetic resonance imaging (fMRI)-compatible robot to study activations during reaching movements suffering from either random goal or random execution errors. Despite very similar kinematics during reaching, activation patterns clearly dissociated goal and execution errors. Second, we compared the neural response with exe-

Received May 10, 2005; revised Aug. 24, 2005; accepted Sept. 17, 2005.

This work was supported by National Institutes of Health (NIH) Grant NS37422, the Human Frontiers Science Program, and Johns Hopkins General Clinical Research Center Grant RPN 02-08-15-03. The mechanical design of the robot was by Michael R. Turner, James Hartwell, and R.S. Robot controllers were designed by Haiyin Chen, Maneesh Dewan, and J.D. The robot was constructed by Jay Burns. We are grateful to the staff of the F. M. Kirby Research Center for Functional Brain Imaging at the Kennedy Krieger Institute for facilitating this study. This Center is funded by NIH/National Center for Research Resources Resource Grant RR15241. Finally, we thank David van Essen, Scott Grafton, Sarah Hemminger, and Maurice Smith for helpful comments.

Correspondence should be addressed to Jörn Diedrichsen, Department of Biomedical Engineering, Johns Hopkins University, 720 Rutland Avenue, 416 Traylor Building, Baltimore, MD 21205-2195. E-mail: jdiedric@jhu.edu.

DOI:10.1523/JNEUROSCI.1874-05.2005

 0270-6474/05/259919-13$15.00/0

cution errors that were attributable to either a visual rotation (kinematics) or a force field (dynamics). Surprisingly, we found that the regions of neural activity were essentially overlapping for these two different types of execution errors.

Materials and Methods

Participants. A total of 39 neurologically healthy volunteers enrolled in the study. Their age ranged from 18 to 45 years (mean of 26 years), with 18 females. All participants were right-handed. Of the 39 volunteers, 10 participated in the behavioral experiment, 13 in imaging experiment 1, and 16 in imaging experiment 2. Each participant took part in only one of the experiments. The Johns Hopkins School of Medicine Internal Review Board approved the study procedures.

Apparatus. In all experiments, participants held onto a two-joint robotic manipulandum, which allowed free two-dimensional movements in the horizontal plane and was capable of applying forces to the hand. For the fMRI studies, a nonmagnetic version of the manipulandum was used (Fig. 1*A*). Forces were applied via air pistons supplied with an air pressure of 100 psi from a compressor outside the MR room. Time constant of the pistons response was ~60 ms to a step input. Linear optical encoders on the elbow and shoulder joint provided position readings with endpoint accuracy better than 0.01 mm to a control computer outside the room. A filter panel in the wall of the scanning room prevented leakage of receptive field noise for both ingoing and outgoing signals. Position and velocity of the hand and the generated forces were recorded at 200 Hz. Numerous pilot studies ensured that the presence and operation of the robotic arm near the scanner bore did not impact the signal-to-noise ratio of the functional data. Targets and visual feedback on the hand position were projected from outside the scanner room onto a back screen, which was viewed by the participants through a mirror.

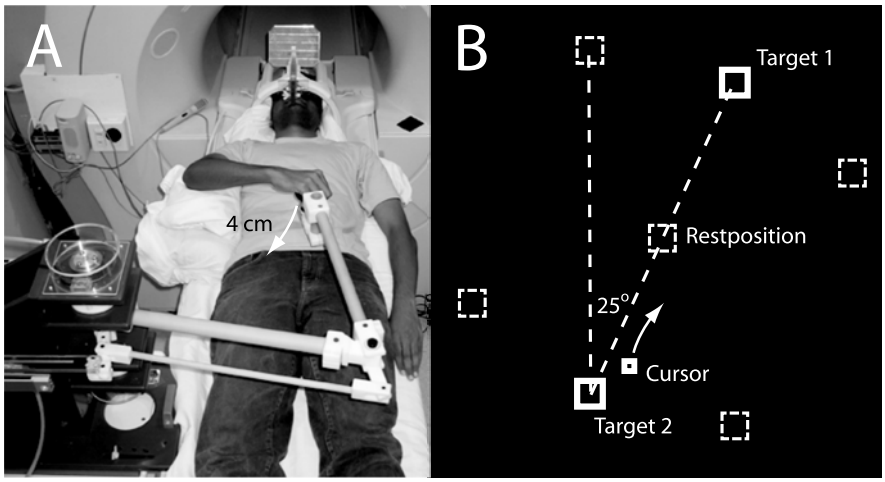

Figure 1. Experimental setup for imaging experiments. ***A***, Participant, for better visibility shown outside the scanner, holds on to a robotic arm and makes 4 cm movements in the horizontal plane (white arrow). ***B***, Visual feedback as viewed by the participant on a back-projection screen. A movement away from the head corresponded to an upward cursor movement. Only the current target and cursor are present on the screen. Dotted target locations indicate the rest position and possible target locations in the target-jump condition.

Behavioral study outside the scanner. The goal of the behavioral study was to test the hypothesis that goal and execution errors would produce different patterns of trial-to-trial adaptation. The study was conducted with the participants ($n = 10$) sitting upright and holding the robot handle with the right hand. The elbow was supported at shoulder height, bringing the arm into the plane of movement. Visual feedback of the hand position was continuously provided by a white 5 mm cursor on a computer screen, which was arranged vertically, 50 cm in front of the participant. Movements were made only in the forward direction; the robot arm brought the hand of the participant passively back to the start position. The target, a red 1.5 cm square, was presented 11 cm above the starting position. When the target turned white, participants were instructed to move the arm quickly and smoothly to the target. Movements with a peak speed between 55 and 80 cm/s were rewarded by a visual "explosion" of the target if they were completed within a time limit. This limit was dynamically adjusted for each participant and condition, such that ~50% of the trials were successful. After each block of 81 trials, feedback was given to the participant concerning the number of achieved explosions.

The experiment began with one training block of normal, unperturbed movements. Before the onset of the second block, participants were given the following instruction: "The apparatus will perturb your movement in different ways. All perturbations are completely random. In all trials, try to move as quickly as you can to the target. If you do not reach the target right away, try to get to the target as fast as possible." The 12 experimental blocks switched sequentially between three conditions: In the visual-rotation condition, the visual feedback was rotated by 0, +12, or −12° around the starting location. In the curl-field condition, a viscous force field (Shadmehr and Mussa-Ivaldi, 1994) of 0, +13, or −13 Ns/m was applied to the hand, exerting forces perpendicular to the movement direction. In the target-jump condition, the target was displaced when the tangential velocity of the hand crossed 4.5 cm/s and had moved at least 1 cm from the initial starting position. The new target positions were located at the same distance and rotated by 0, +12, or −12° around the starting position. In all three conditions, the direction of perturbation was randomly selected with equal probability.

State space model of trial-by-trial adaptation. We asked whether target errors (attributable to target jump) or execution errors (attributable to visual rotation or force field) produced distinct patterns of adaptation as reflected in the feedforward motor commands in the subsequent trial. We used a state-space model to quantify the patterns of trial-by-trial adaptation for the behavioral data collected outside the scanner (Thoroughman and Shadmehr, 2000; Donchin et al., 2003; Wainscott et al., 2005):

$$\begin{aligned} y_n &= Du_n - z_n + \varepsilon_n \\ z_{n+1} &= z_n + By_n + \eta_n \end{aligned} \quad (1)$$

The error on trial n is noted by y_n and is expressed as a function of the perturbation u_n, the internal state of the system z_n, and the output noise ϵ_n. The error in each trial was measured as the angle between the line connecting the starting point and the hand position at 200 ms and the line connecting the starting point and the final hand position. The parameter D indicates how much angular error is caused by a perturbation in a naive participant ($z_n = 0$). For the force-field condition, this parameter relates to the stiffness of the arm, whereas in the visual-rotation and target-jump conditions, this parameter is close to one, because a 12° rotation of target or feedback induces an equally sized error. The second equation states that the internal state (z) changes by a certain proportion of the experienced error, in which the amount of change is determined by the adaptation rate B and by a random noise term, the state noise η_n. The parameters D and B and the noise variances σ^2_ϵ and σ^2_η were estimated for each participant and condition using an expectation-maximization algorithm.

Scan acquisition. Data were acquired on a 3 T Philips Intera system (Philips Medical Systems, Best, The Netherlands). For functional scans, we used an echo planar imaging (EPI) sequence with sensitivity-encoded MRI (Pruessmann et al., 1999) and a sensitivity-encoding factor of 2. The whole brain was covered in 37 axial slices (3 mm thickness; 0.5 mm gap; repetition time, 2 s), each of which was acquired as an 80 - 80 matrix (field of view was 24.0 × 24.0 cm), with a voxel size of 3 × 3 × 3.5 mm. The image was reconstructed to 128 × 128. Each scan consisted of six dummy images that were discarded and 176 (experiment 1) or 144 (experiment 2)

data images. T1-weighted structural images were acquired with $1 \times 1 \times 1$ mm resolution using a magnetization-prepared rapid-acquisition gradient echo sequence without sensitivity encoding for higher signal-to-noise ratio.

Artifacts. fMRI studies of overt arm movements with a robotic device pose significant technical challenges. At 3 tesla, head movements of <1 mm can increase the noise variance of individual images by a factor of 3 (Diedrichsen and Shadmehr, 2005). Therefore, all participants used a custom-fit bite bar for head stabilization.

Even with the head perfectly stabilized, the dislocation of a mass near, but outside of, the head coil can induce strong signal changes in EPI images. We confirmed this observation by placing a water-filled phantom into the head coil and positioning another water bottle at 30 cm distance below the head coil, either on the left or right side of the bed. Significant signal differences were observed depending on the position of the external bottle.

To address this issue for the current study, the movements were only 4 cm long, in contrast to 11 cm in the behavioral study, and involved mostly the elbow joint, minimizing the amount of mass that was displaced with the movement. The position of the hand during the acquisition of baseline images was located between the two target positions. Therefore, the average hand position during movement phases and during baseline phases was the same, and locally linear components of a static distortion effect would be averaged out.

To test whether nonlinear changes induced a bias into the data, we directly studied the influence of hand position on the fMRI signal. For 21 of 29 participants, we included a scan in which they were instructed to move the hand to the rest position, target 1, and target 2 and hold each position for 20 s. Each position was repeated four times. We then computed the difference between images taken when the hand was at a target versus when the hand was at the rest position. If the position-dependent artifact biased our results, this difference image should correlate with any movement versus rest contrast image.

Although this approach tested for the possibility that the artifact biased our results, it remained possible that the movements induce noise and increase the variance of the observations, leading to a loss of sensitivity. We therefore developed a new statistical technique with which the noise variance in each image can be estimated in an unbiased manner, using restricted maximum likelihood estimation (Diedrichsen and Shadmehr, 2005). In a weighted least-squares approach, these images can be down weighted by the inverse of that variance, minimizing their influence on the result.

Imaging procedures. All participants underwent a training session 1–5 d before scan acquisition. The session was conducted in a mock scanner with a setup identical to the real scanning environment. Participants familiarized themselves with the bite bar and learned to perform movements in the scanner. During training, participants completed four blocks of 80 trials of unperturbed movements. Depending on the experiment, the practice also included reaching trials in a resistive field or in the first visual control conditions (see below).

During the scan session, participants lay in a supine position, used a custom-fit bite bar, and grasped the robot handle with their right hand while the elbow was supported by a cushion (Fig. 1*A*). The center target was adjusted for each participant such that his or her hand was positioned right above the navel. Movements were performed in the horizontal plane.

To optimize experimental power, we chose a block design with task phases of 10 movements. In these task phases, a new target appeared every 2 s. There were two possible target positions, diagonally above or below the starting position (Fig. 1*B*), arranged at an angle such that movements between targets 1 and 2 involved mostly elbow flexion and extension. Whereas participants were moving in only one direction in the behavioral study, we chose to have participants move in both directions in the imaging studies to avoid neural activity related to the passive return of the arm to the starting position. Thus, the endpoint of each movement, which depended on the perturbation on that trial, became the starting position for the next one. This constraint precluded the possibility of using the state space model to measure the trial-by-trial adaptation rate, because we cannot distinguish between the history of perturbations and biomechanical difference between different movement directions. However, in a pilot study on $n = 8$ subjects, using constant force fields with interspersed catch trials and two movement directions, we observed a similar trial-to-trial adaptation inside the scanner as usually found outside the scanner (Thoroughman and Shadmehr, 2000).

Each trial began with the presentation of the target. Participants were instructed to move the cursor to the target immediately on appearance. Each movement had to end in the target, and a movement was considered successful if the hand reached a velocity of >20 cm/s during the movement and the cursor was brought into the target in time. A visual target explosion indicated success. The movement duration criterion was flexibly adjusted such that the number of explosions was equal among all conditions. The cursor was continuously visible. The first movement of a block consisted of a 2 cm movement toward one of the targets, followed by eight 4 cm movements back and forth between the two targets and finally by a 2 cm movement back to the starting position. After this block of 10 movements (20 s), there was a 14 s rest phase, in which participants were instructed to remain motionless and fixate the cursor. The experiment design focused on making the kinematics of the reaching trials as similar as possible between the various conditions (target jump, visual rotation, and curl field).

Imaging experiment 1. In this experiment ($n = 13$), we compared the activation patterns attributable to target errors (target jump) versus execution errors (visual rotation). In the target-jump condition, the target was displaced to a new location when the arm moved faster than 4.5 cm/s. The new location was at the same distance from the start of the movement as the old location rotated clockwise or counterclockwise by 25° (Fig. 1*B*). Displacements occurred randomly in six of the middle eight movements, whereas two movements were unperturbed. In the visual-rotation condition, visual feedback was rotated either clockwise or counterclockwise around the starting position. To avoid discontinuous displacements of the cursor, two trials were performed under the same rotation condition. Interspersed in the middle eight movements were two unperturbed movements, such that the center of rotation could change within a task block from target 1 to target 2. The amount of rotation was 25° for the first five participants, such that the size of the errors was comparable with the target-jump condition. In this case, movement durations were longer in the visual-rotation condition (Table 1). Thus, for the last eight participants, the amount of rotation was adjusted, such that movement duration was approximately matched between the two conditions.

We also included two visual control conditions without hand movements to account for differences in visual stimulation, shifts of attention, and eye movements. In the first visual control condition, the sequence of target appearances mimicked exactly the visual-rotation condition (including target explosions). In the second visual control condition, targets were displaced randomly on 6 of the 10 trials. The timing of displacements and possible explosions were based on behavioral data from the target-jump condition. Participants were instructed to follow these targets with their eyes as under normal movement conditions but not to move their hand. As an instructional cue, the cursor turned blue in these conditions and remained stationary at the center. We also included a normal movement condition in which reaches were performed without perturbation.

Imaging experiment 2. In this experiment ($n = 16$), we compared two different forms of execution errors: one attributable to visual rotation and another attributable to a force field. The visual-rotation condition was identical to experiment 1, but the rotation was set to $\pm 25°$. In the curl-field condition, a viscous curl field (± 12 Ns/m) was applied to the hand. The force field was turned off when the hand velocity dropped below 4.5 cm/s. The experiment also included a normal movement condition between the two standard targets. For half of the participants, a resistive-field condition was added, in which a viscous force was applied opposite the principal movement direction. The resistive field was designed to make the integrated shoulder and elbow torque equal to the curl-field condition, approximately equating the total force produced in the two conditions.

Movement data analysis. Velocity data were smoothed with a Gaussian

Table 1. Average movement parameters (SD) for the conditions of the imaging experiments 1 and 2

	Normal movement	Visual rotation	Condition curl field	Target jump	Resistive field
Experiment 1 (participants 1–5)					
Movement duration (ms)	417 (26)	614 (68)		569 (57)	
Movement error (degrees)	4.6 (0.6)	25.1 (3.9)		25.5 (2.1)	
Movement length (cm)	4.3 (0.4)	5.9 (0.5)		5.4 (0.5)	
Experiment 1 (participants 6–13)					
Movement duration (ms)	481 (26)	576 (68)		559 (57)	
Movement error (degrees)	3.2 (0.6)	19.2 (3.9)		25.2 (2.1)	
Movement length (cm)	6.6 (0.4)	5.7 (0.5)		5.9 (0.5)	
Experiment 2					
Movement duration (ms)	422 (41)	648 (45)	631 (49)		491 (64)
Movement error (degrees)	6.5 (1.8)	25.3 (1.6)	25.4 (4.6)		6.6 (2.3)
Movement length (cm)	4.8 (0.5)	6.7 (0.7)	6.9 (1.2)		4.4 (0.1)

Movement duration (in milliseconds) encompasses all corrective submovements. Movement error is the absolute angular deviation of the initial movement direction (200 ms) from the final movement direction. This measure is calculated only for the perturbed movements, whereas the other parameters are averaged over all movements (except the first and last movement of a 10 movement block).

kernel of 10 ms full-width half-maximum. Movement initiation was defined as the time when the hand velocity crossed the threshold of 2 cm/s and sustained this speed for at least 100 ms. Movement termination was the last time the hand velocity fell below 2 cm/s for that trial. Thus, our measure of movement duration included all corrective submovements. All movements stopped in the target. Movement length was the total path traveled by the hand in that trial. The angular error was computed as the angle between the line connecting start point and endpoint of the movement, with the line connecting the start position and the hand position at 200 ms.

Imaging data analysis. Functional imaging data were analyzed using Matlab (MathWorks, Natick, MA) and SPM2 (Wellcome Department of Cognitive Neurology, London, UK) (Friston et al., 1999). For preprocessing, data were temporally realigned to correct for the sequence of slice acquisition and then spatially aligned to the first scan with a six-parameter rigid-body transform. Data were high-pass filtered with a cut-off frequency of $1/128$ s to remove slowly varying trends and normalized by a single constant for each scan. The data of each voxel was fitted with a linear model that contained a separate regressor for each task phase. Each regressor was a boxcar function spanning a block of 10 movements, convolved with an estimated hemodynamic response function. The shape of this function was estimated based on a set of preliminary experiments on eight subjects. To control for possible noise artifacts in the data, we used a weighted least-squares approach down weighting images with high noise variance (Diedrichsen and Shadmehr, 2005). The resulting coefficient for each regressor was then transformed into percentage signal change by dividing the peak of the predicted response by the mean signal intensity for that voxel.

We pursued two different strategies for intersubject spatial normalization. For subcortical areas, we normalized the individual anatomies to the Montreal Neurological Institute (MNI) template using a high-dimensional nonlinear transform (Ashburner and Friston, 1999). For this purpose, the functional data were smoothed with a 6 mm Gaussian kernel. The functional data from the cerebellum was visualized using a surface-based representation of an individual cerebellum (Van Essen, 2002). For cortical areas, we used the software Caret [http://brainmap-.wustl.edu/caret (Van Essen et al., 2001)] to segment the left and right hemisphere, reconstruct the cortical surface, and inflate each hemisphere to a spherical representation. The individual spheres were then aligned using six anatomical landmarks to the new population-averaged, landmark- and surface-based atlas (Van Essen, 2005). The unsmoothed functional data for each condition and participant were then projected onto this atlas surface and smoothed on the surface with an iterative procedure using local averaging (10 iterations, strength 1). Group inferences were made from the two-level random-effects analysis from these smoothed images. The statistical threshold was fixed at $\sqrt{n}$ for each experiment (effect size of 1). To correct for multiple comparisons, we applied random-field theory (Worsley et al., 1996) to the two-dimensional statistical maps (Diedrichsen, 2005) and used clusterwise p values for the given t threshold.

Results

We began with a psychophysical experiment to compare consequences of random target errors (target jump) with random execution errors (visual rotation or force fields). Regardless of the type of perturbation, all movements exhibited smooth corrections (Fig. 2*A*). The similarity in on-line corrections after target jumps or visual rotations is apparent in the hand velocity perpendicular to the main movement direction (Fig. 2*B*). Relative to when the hand left the starting position, the correction began at 171 ms for the target-jump condition and at 193 ms for the visual-rotation condition and followed similar time courses. The onset of this correction occurred before the main forward movement had ended (Fig. 2*C*). Notice that the corrections in the curl-field condition cannot be easily assessed using this measure attributable to the interaction between perturbation, arm stiffness, and short-loop reflexes.

Despite the kinematic similarities in the on-line correction, goal and execution errors triggered different adaptive responses. We quantified adaptation by estimating the effect of errors experienced in one trial on the internal state of the system that produced the motor commands in the subsequent trial (Eq. 1). The adaptation rate B specifies the proportion of error in trial n that consistently affects the internal state for trial $n + 1$. The strength of the model is that it allows for measurement of adaptation even when perturbations are random and do not lead to sustained changes in behavior.

We fit Equation 1 to the sequence of trial-by-trial errors produced by each subject as they experienced the random perturbations. Figure 2*D* shows the estimates for adaptation rates in the force-field, visual-rotation, and target-jump conditions. Replicating previous results (Donchin et al., 2003), the adaptation rates for the curl-field condition were on average 0.15. We also found similar responses to random visual-rotation errors (curl field vs visual rotation, $t_{(9)} = 2.13$; $p = 0.062$). In contrast, the errors in the target-jump condition produced significantly smaller adaptation (target jump vs visual rotation, $t_{(9)} = 11.32$; $p < .001$).

We do not claim that participants cannot learn from target errors. In fact, if the target error was such that the target was displaced in a systematic manner, participants would likely learn to change their motor plan accordingly. The main point is that trial-by-trial learning remained substantial in response to randomly applied visual or force perturbations, whereas little or no adaptation was found in response to random target jumps, indicating separate mechanisms for adaptation.

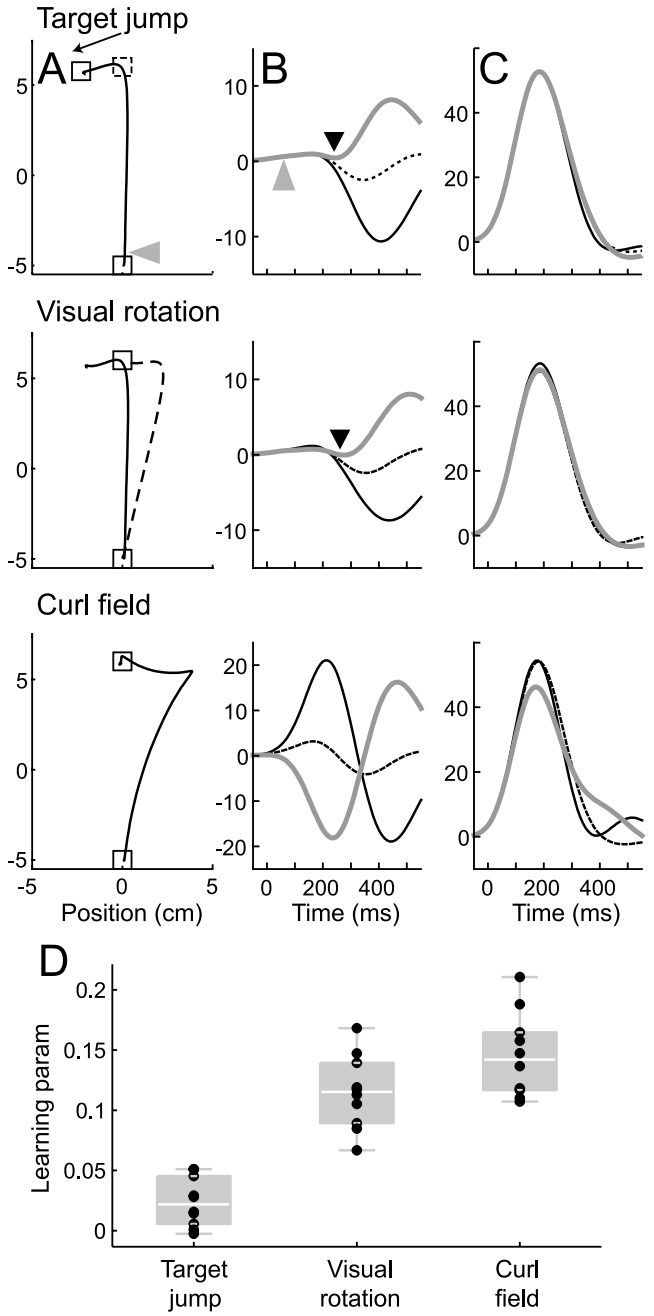

Figure 2. Results of the behavioral experiment. ***A***, Average hand position trace (solid line) and cursor position trace (dashed line) in the target-jump, visual-rotation, and curl-field conditions. All movements start at the lower box. The gray triangle indicates average position and time of target jump. Hand velocities (in centimeters per second) in the lateral direction (***B***) and in the forward direction (***C***) for trials perturbed to the left (black line), to the right (gray line), and unperturbed trials (dashed line). The black triangle marks the average onset of the correction. ***D***, Trial-to-trial adaptation rater estimated from the state-space model (Eq. 1; see Materials and Methods). The dots plot the estimates for individual participants.

In the imaging experiments, we exploited this difference in the adaptive response and studied the neural signatures of execution and target errors. We reasoned that any brain region that undergoes adaptive changes in response to execution errors must receive this error signal. Because the blood oxygenation level-dependent (BOLD) signal is likely driven to a large degree by presynaptic activity (Logothetis, 2003), these regions should show increased activity when execution errors occur.

We carefully tested our data for artifacts that could possibly arise from overt arm movements in the MR environment. First, overt head movements were successfully reduced using the custom-fit bite bar. The average translation between two adjacent images was 0.1 mm, accumulating to an average maximal translation over the course of the whole experiment of 1.5 mm. Second, we tested whether the position of the arm induced a bias into the functional data: The average correlation between the effect of hand position, as determined by the additional control scan, and our movement versus rest contrast was 0.03 (SD of 0.17). Thus, no consistent bias attributable to changes in arm position was present. Finally, we estimated the noise variance for each image. Although our method identified head movement, swallowing, blinking, and other related artifacts (Diedrichsen and Shadmehr, 2005), we did not find increased noise variance during arm movement blocks compared with rest blocks. On the contrary, the noise variance was estimated to be 5% lower during arm movement and 8% lower during visual control conditions than during rest blocks. This suggests that participants showed more head movement, swallowing, and blinking when not being engaged in a task. In comparison, noise arising from the arm movements themselves appeared to be modest. The imaging data are available in the Surface Management System Database (http://sumsdb.wustl.edu:8081/sums/directory.do?id = 6406115).

Experiment 1: target errors versus execution errors

In experiment 1, we compared neural activity in the target-jump and visual-rotation conditions. Because neural activity is likely to be affected by kinematics of the reach, we attempted to match as many variables as possible for the planned comparisons. We considered three variables: movement duration, angular error, and movement length. We found that it was not possible to match all three variables simultaneously in the two conditions. Therefore, we compromised, divided our subjects into two groups, and attempted to match different movement parameters in different groups. In the first five subjects, we positioned the targets to equate the angular error in the two conditions (Table 1). This produced average movement errors that differed by only 0.4°, but the length was 5 mm and the movement duration was 45 ms longer in the visual-rotation condition. For the subsequent eight participants, we adjusted the visual rotation angle dynamically to match movement length and duration between conditions. The average rotation angle was 20.2° compared with a 25° displacement in the target-jump condition. This led to relatively well matched kinematics: the movement lengths and duration differed by only 1.4 mm and 17 ms, respectively (Table 1). For the imaging results, we averaged the first five and last eight participants together. However, for each region, we checked that the results were still significant when the difference in movement duration, length, or angular error between conditions was used as a covariate in the across-subject analysis. All reported regions passed these tests.

To compare neural activity in the visual-rotation and target-jump conditions, we also had to consider important differences in terms of visual stimuli and the resulting eye movements. We included two visual control conditions. In the visual control 1 (C1) condition, we programmed a sequence of saccade targets that were identical in timing and position to the visual-rotation condition. In the visual control 2 (C2) condition, the programmed sequence of saccade targets matched the target-jump condition. Participants were instructed to saccade to every target while holding the hand still. In the control conditions, we did not show any cursor movements because observation of reach errors in force fields, without any overt movements, can lead to adapta-

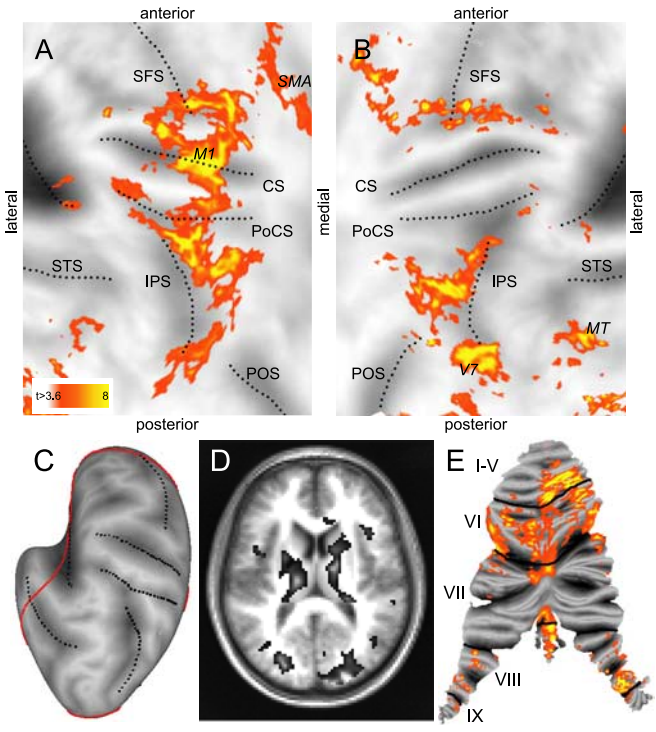

Figure 3. Population-averaged activity related to normal reaching movements compared with rest on a flattened representation of the left (***A***) and right (***B***) cortical hemisphere is shown. The lateral and parts of the medial surface of parietal and frontal lobe are shown: grayscale indicates sulcucal depth with sulci shown in dark gray, averaged across participants. SFS, Superior frontal sulcus; CS, central sulcus; PoCS, postcentral sulcus; IPS, intraparietal sulcus; STS, superior temporal sulcus; POS, parieto-occipital sulcus; MT, middle temporal area. ***C***, Sulci (black lines) and the border of the flattened representation (red line) on an inflated representation of the left hemisphere. Average movement-related activity in basal ganglia and thalamus (***D***) and on a flattened representation of the cerebellum (***E***) is shown. Roman numerals denote cerebellar lobules according to the Larsell notation (Schmahmann et al., 2000). All maps are thresholded at $t_{(13)} > 3.61$.

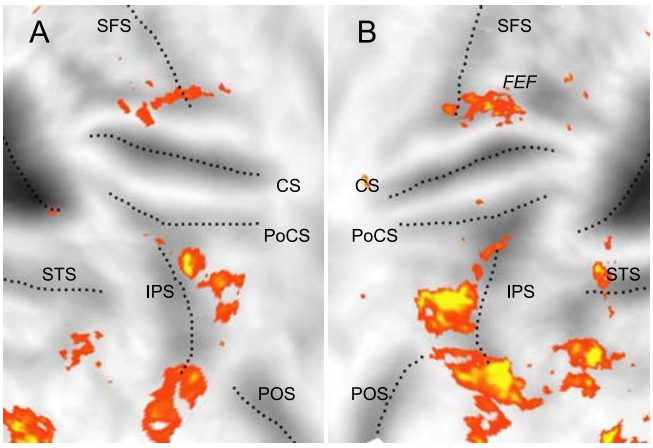

Figure 4. Averaged activity in the visual control condition 2 versus rest on a flat representation of the left (***A***) and right (***B***) cortical hemispheres is shown. Threshold is $t_{(13)} > 3.61$. FEF, Human frontal eye field. Other abbreviations as in Figure 3.

tion (Mattar and Gribble, 2005). Although we did not monitor eye movements during imaging, we confirmed in a control study that, in visual control and movement conditions, participants reliably made a single saccade to every new target and an additional saccade when the target jumped. We also confirmed in the control study that, in the normal-movement and the visual-rotation conditions, despite errors, participants maintained fixation of the target during the entire course of the reach (Neggers and Bekkering, 2001). Therefore, eye movements were well matched between the reach and the respective control conditions.

Figure 3 shows the reach-related activity (reach vs rest) on a surface atlas representation of the cortical hemispheres. The arm area of the left primary motor cortex showed the highest peak of activity. Activity was also observed bilaterally in premotor cortex and parietal areas along the postcentral sulcus and the medial bank of the intraparietal sulcus (IPS), extending backward into the intersection of IPS and the transverse occipital sulcus (IPS/TOS). The latter area is likely equivalent to V7 and V3a (Tootell et al., 1998). An area located in the ascending branch of the posterior inferior temporal sulcus, likely the human homolog of the middle temporal area (Sunaert et al., 1999), was also consistently activated, as well as lower level visual areas (data not shown). Subcortical activity (Fig. 3*D*) was also observed in the striatum, globus pallidus, and thalamus. In the cerebellum, we found reach-related activity mostly in ipsilateral anterior cerebellum (V) extending into lobule VI and bilaterally in lobule VIII (Fig. 3*E*). These cerebellar areas have been shown to have reciprocal connection with primary motor cortex (Kelly and Strick, 2003).

The activation patterns in the two visual control conditions were similar to each other, with generally larger activations in the second visual control condition. Figure 4 shows the C2 versus rest contrast, which revealed a bilateral network consisting of the precentral sulcus, an area that is thought to be the human homolog of the frontal eye fields (Koyama et al., 2004; Curtis et al., 2005), and areas in the medial bank of the IPS. Our results are consistent with the idea that the human homolog of the lateral intraparietal area is situated in the medial bank of the intraparietal sulcus (Corbetta et al., 1998; Sereno et al., 2001; Koyama et al., 2004; Schluppeck et al., 2005). The left thalamus was the only subcortical area that showed increases in BOLD signal in the visual control conditions.

To arrive at a contrast that reveals neural activity specifically coding for either target errors or execution errors, we assumed that signal changes during normal reaching (N) were attributable to two sources: activity arising from the execution of the reach movement (M_1), and activity related to the visual stimulation, attention shifts, and eye movements (E_1). That is,

$$\mathrm{N} = M_1 + E_1 \tag{2}$$

In contrast, in the visual-rotation condition (VR), we assumed that signal changes were attributable to three sources: neural activity related to the reach and on-line correction (M_2), activity arising from the visual stimulation and saccades (E_1), and activity related to the processing of the kinematic execution error (ϵ_K). That is,

$$\mathrm{VR} = M_2 + E_1 + \varepsilon_K \tag{3}$$

In the target-jump condition (TJ), the activity related to reach kinematics (M_2) was approximately the same as in the visual-rotation condition (Table 1). The target jump, however, caused an additional saccade compared with the normal condition. Thus, signal increases observed in the target-jump condition could be caused by the additional eye movement (E_2), as well as by the processing of target errors (ϵ_T):

$$\mathrm{TJ} = M_2 + E_2 + \varepsilon_T \tag{4}$$

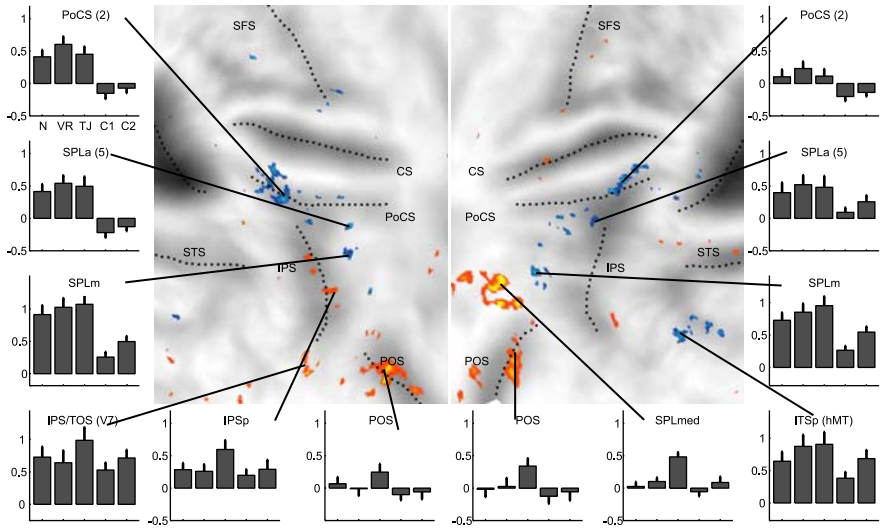

Figure 5. Statistical *t* map of areas activated more attributable to execution errors that lead to adaptation of internal models (blue) or more attributable to target errors that arise from a change in the reach target (red). Shown is the interaction contrast of Equation 5 at a threshold of $t_{(13)} > 3.61$. Bar graphs with the percentage signal change relative to rest from significant cluster are shown on the margins. Abbreviations as in Figure 3

The two visual control conditions C1 and C2 were designed to detect activity attributable to eye movements and visual stimulation, i.e., C1$\sim E_1$ and C2$\sim E_2$. Therefore, to detect neural activity that distinguished the two kinds of error, we used the following contrast:

$$\varepsilon_T - \varepsilon_K \sim (\mathrm{TJ} - \mathrm{C2}) - (\mathrm{VR} - \mathrm{C1}) \quad (5)$$

To exclude spurious activations, we restricted our search region to task-related areas. These were defined as areas that showed a net positive signal change, averaged across all movement conditions. This lenient criterion led to a large search region that only excluded the inferior prefrontal and inferior temporal cortices. Within this search area, we identified voxels in which the above contrast was significant at a threshold of $t_{(12)} = 3.61$. Clusterwise *p* values, derived using Gaussian field theory (Friston et al., 1994), were then used to correct for the size of the search region.

The red areas in Figure 5 (see also Table 2) indicate clusters above threshold in which activity was driven preferentially by target errors, and the blue areas indicate clusters that were driven more by execution errors. In the cerebral hemispheres, areas that were more activated by target errors were exclusively in the posterior parietal cortex. In the left hemisphere, target errors activated multiple regions in the depth of the intraparietal sulcus, only one of which was significant. This cluster [the posterior IPS (IPSp)] showed activity related to eye movements and combined arm and eye movements but was especially active when the reach goal changed. A number of regions in the medial wall of the right superior parietal lobe (SPLmed) and bilaterally in the parieto-occipital sulcus (POS) showed large increases in activity attributable to target errors. These areas were characterized by a very small signal change for normal movements. Finally, we also found an area between the IPS and the TOS involved in the detection of the target error. This area is likely a homolog of V3A or V7 (Tootell et al., 1998; Medendorp et al., 2005; Schluppeck et al., 2005).

In contrast to the target errors, the execution errors attributable to visual rotation activated regions more anterior in the parietal lobe (Fig. 5, blue). Clusters with very strong activity were found bilaterally in the postcentral sulcus, on the boundary between Brodman area 2 and area 7 (Grefkes et al., 2001). In both hemispheres, the activity extended in the superior-posterior direction into area 5 (Fig. 5*A*, SPLa). Indeed, the area 5 cluster in the left hemisphere had the highest negative *t* value in the entire map, suggesting a strong drive attributable to execution errors. None of the clusters in area 5 and postcentral sulcus were driven by the visual control conditions. In contrast, the more posterior clusters in the middle SPL were activated considerably in the visual control conditions. The interaction contrast (Eq. 5) indicated involvement in execution errors, despite the fact that these clusters were more active during the target-jump condition than during the visual-rotation condition. However, the difference between the two visual control conditions was significantly larger, suggesting that stronger activation during execution errors was overlaid with some weaker eye-movement-related activity.

To look for subcortical correlates of goal and execution errors, we used a search area confined to all subcortical and cerebellar voxels with movement-related activity. In this search region, we found only two significant clusters (using clusterwise *p* values, corrected for the search volume) activated attributable to target errors: a cluster in the left striatum ($p = 0.03$) and a cluster in the right striatum ($p < 0.001$) (Fig. 6*A*). We also found a goal-error-related cluster outside the gray matter in an area between superior colliculus, temporal lobe, and anterior cerebellum. Given the location of this cluster, we believe it to be an artifact. Importantly, we found no significant clusters in the basal ganglia, the cerebellum, or any other subcortical region in which execution errors produced larger increases in activity than target errors. The biggest cluster related to execution errors were two small sites in lobule VIII (Fig. 6*B*) of the cerebellum (MNI, −16, −70, −56; MNI, 22, −78, −50), but both of these clusters were far from significant ($p = 0.418$; $p = 0.294$). To better reveal the activity patterns in the movement-related areas in basal ganglia and cerebellum, we used regions of interest (ROIs) based on the averaged anatomical image outlining the putamen, caudate, globus pallidus, thalamus, cerebellar hemispheres I–V, VI, and VIII, vermis V and VI, and dentate nucleus. In each region, we identified movement-related voxels based on the within-participant fixed-effects analysis ($t_{(12)} = 1.64$; $p = 0.05$). The proportions of movement-related voxels for each ROI are noted in Figure 6*C*. For example, approximately half of the voxels in both the left and right putamen, but ~80% of the voxels in the right cerebellum lobule V, were found to be movement related. Next, we averaged the percentage signal change in movement-related voxel in each ROI across subjects. Thus, our selection criterion for voxels (anatomical criteria + movement > rest) was independent of the contrast of interest (Eq. 5).

The ROI analysis confirmed the results of our voxel-based analysis. Of all subcortical ROIs, only the left putamen ($t_{(12)} = 2.44$; $p = 0.03$), the right putamen ($t_{(12)} = 3.42$; $p = 0.005$), and the right caudate ($t_{(12)} = 2.22$; $p = 0.004$) showed a significant interaction contrast (Eq. 5), indicating a preferential involvement in target errors. Strikingly, execution errors led to a sup-

Table 2. Anatomical areas that showed a significant interaction contrast (Eq. 5) on a clusterwise level in experiment 1

					PALS		MNI		
Area	Side	Extend (mm^2)	Peak t	P (cluster)	Latitude	Longitude	x	z	y
More activated during target errors									
IPSp	L	39	4.71	0.028	1	157	−28	−63	54
SPLmed	R	112	7.71	<0.001	−30	131	7	−65	60
SPLmedp	R	71	7.79	<0.001	−33	143	11	−72	52
IPS/TOS (V3a/V7)	L	70	7.66	<0.001	−22	−180	−22	−87	22
POS	L	184	9.31	<0.001	−60	167	−16	−73	21
POS	R	80	4.86	<0.001	−49	152	17	−71	35
POSinf	R	41	5.50	0.019	−80	160	14	−55	14
More activated during execution errors									
PoCSa (2)	L	167	−6.11	<0.001	51	139	−55	−22	51
PoCSp (2/7)	L	128	−6.51	<0.001	41	151	−45	−31	45
PoCS (2)	R	60	−6.12	0.025	48	145	51	−23	50
PoCS (2)	R	39	−4.95	0.033	66	152	62	−12	39
SPLa (5)	L	17	−7.08	0.78	8	134	−30	−45	66
SPLa (5)	R	41	−4.16	0.026	24	147	37	−38	52
SPLm	L	50	−4.59	0.003	3	141	−32	−53	64
ITS (hMT)	R	100	−5.61	<0.001	−2	−144	46	−72	3

Height threshold was $t_{(12)} = 3.61$; $p = 0.002$ (uncorrected). The total search volume was 110,156 mm^2 (2869 resels), with an estimated smoothness of full-width half-maximum of 6.2 mm. The expected size of random clusters was 5.5 mm^2. All area sizes are calculated on individual surfaces and averaged (Diedrichsen, 2005). The SPLa cluster on the left side was not significant but was reported because it contained the highest t value, and we found a homologous area activated on the right side. The location of the maxima is listed in latitude/longitude for the population-averaged, landmark- and surface-based atlas (Van Essen, 2005) and the template of the MNI. L, Left; R, right; IPSp, posterior intraparietal sulcus; SPLmedp, middle posterior superior parietal lobe; POSinf, inferior parieto-occipital sulcus; PoSC, postcentral sulcus; PoCSa, anterior postcentral sulcus; PoCSp, posterior postcentral sulcus; SPLa, anterior superior parietal lobe; SPLm, medial superior parietal lobe; ITS (hMT), inferior temporal sulcus (human homolog of MT).

pression of activity in the putamen compared with normal movements (left putamen, $t_{(12)} = -2.13$, $p = 0.054$; right putamen, $t_{(12)} = 3.29$, $p = 0.006$). In contrast, both execution and target errors significantly activated the right anterior cerebellum (VR-N, $t_{(12)} = 2.69$, $p = 0.019$; TJ-N, $t_{(12)} = 3.26$, $p = 0.006$).

In summary, random target errors produced significantly increased activity in the posterior aspects of the superior parietal cortex, including areas along the left intraparietal sulcus (IPSp and V7), as well as regions in the medial wall (SPLmed, POS). Furthermore, target errors produced increased activity in the putamen and caudate nuclei of the basal ganglia. Random visual rotations resulted in reaches that had kinematic errors comparable with the target-jump condition. However, these execution errors led to large activity in the somatosensory cortex and the anterior aspects of the superior parietal cortex (area 5). The cerebellum showed signal increases for both types of errors.

Experiment 2: kinematic versus dynamic execution errors

The second goal of our investigation was to compare areas involved in the correction of kinematic and dynamic errors. It has been suggested that the computations underlying the control of reaching differentiate between kinematics and dynamics (Atkeson, 1989; Flash and Sejnowski, 2001; Shadmehr and Wise, 2004). First, the visual difference vector between the hand and the target is translated into a kinematic plan, i.e., a plan of how the joint angles have to change to bring the hand to the target. In a second step, the kinematic plan has to be transformed into the torques and muscle commands required to make the desired movement. It has been hypothesized that kinematic and dynamic errors lead to adaptation in two separate inverse models (Krakauer et al., 1999). Based on this hypothesis, we predicted that kinematic and dynamic errors should activate neighboring but spatially separate regions of the motor system.

Experiment 2 was designed to test this hypothesis. We identified regions that responded to kinematic errors (ϵ_K) or dynamic errors (ϵ_D) by comparing the neural response in the visual-rotation (VR) or the curl-field condition (CF) with normal, unperturbed movements (N). Additionally, this contrast was also sensitive to neural responses attributable to the additional movement corrections compared with normal movements ($M_2 - M_1$).

$$\mathrm{VR}-\mathrm{N} = \epsilon_K + (M_2 - M_1) \quad (6)$$

$$\mathrm{CF}-\mathrm{N} = \epsilon_D + (M_2 - M_1) \quad (7)$$

The strength of the force field was adjusted so that the reaches in the two conditions were similar in terms of angular error, movement length, and movement duration (Table 1). Thus, a direct comparison between the two conditions would reveal regions that preferentially respond to either dynamic or kinematic errors. The arm torques needed to correct for the perturbation, however, are higher in the curl-field condition than in the visual-rotation condition, which could lead to higher activity in the curl-field condition. For half of the participants, we therefore added a resistive-field condition to match the additional torques required in the curl-field condition. By comparing this condition to normal movements, we determined which areas were sensitive to the higher torque requirements in the absence of errors.

Compared with normal movements (reach without perturbations), there were significantly activated clusters for both the visual-rotation and curl-field conditions in the arm area of the left primary motor cortex (M1), bilaterally in the secondary somatosensory cortex (SII), and bilaterally in SI along the postcentral sulcus (Fig. 7*A*,*B*). We also found a significant cluster in the dorsal premotor cortex for the visual-rotation condition. In experiment 1, we had found slightly higher response to execution than to target errors in exactly the same region (Fig. 5), although these results were not significant on a clusterwise level.

Although kinematic and dynamic errors activated primarily overlapping areas, it appeared that the activity in the visual-rotation condition involved more posterior regions of the parietal cortex, particularly in area 5. To test for the difference between visual-rotation versus curl-field condition, we began with a mask that included regions that were more active during movement than during rest. We then looked within this area for re-

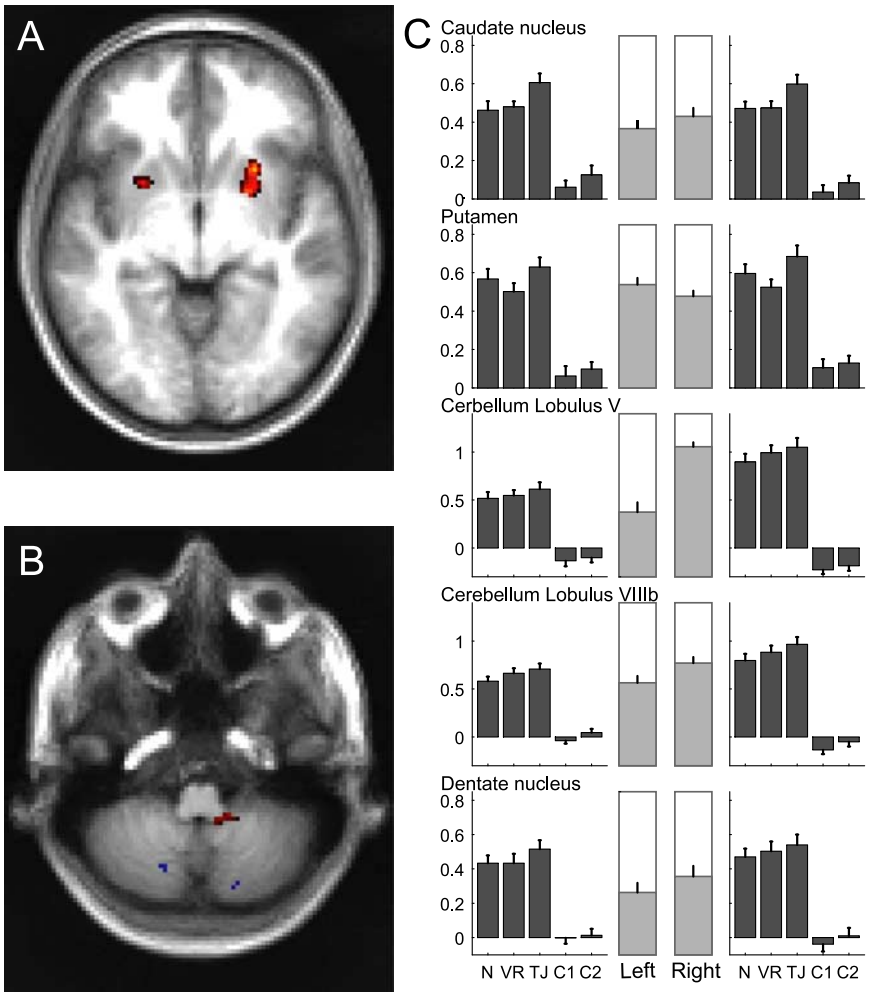

Figure 6. Interaction contrast (Eq. 5) for the subcortex. ***A***, Left ($p = 0.031$) and right ($p < 0.001$) striatum show a stronger response to goal errors than to execution errors. ***B***, No significant sites were found in the cerebellum (see Results). ***C***, Activation in anatomically defined ROIs. Results for symmetric left and right ROIs are shown next to each other. The middle bars show the proportion of each ROI that was identified as task related (average movement > rest; $p < 0.05$ uncorrected). The bar graphs show percentage signal change averaged only over task-related voxel for normal movement (N), visual-rotation (VR), target-jump (TJ), visual control 1 (C1), and visual control 2 (C2) conditions.

gions that were activated attributable to execution errors, i.e., (visual rotation + curl field)/2 versus normal movement. Within this final search region, we identified clusters that showed significant differences between the curl-field and visual-rotation conditions. Contrary to our prediction, we found no significant clusters that showed higher increases in activity in response to dynamic errors compared with kinematic errors of the same size. Rather, dynamic errors only produced neural activity in regions that were also activated by kinematic errors. However, there was a single cluster in area 5 of the left hemisphere that was significantly more active in response to kinematic errors than to dynamic errors (corrected $p = 0.029$; MNI, −26, −45, +68).

The resistive-field condition (compared with normal movements) led to significant activation restricted to the ipsilateral M1 and the bilateral SII (Fig. 7*A*). We therefore have to consider the possibility that the activity observed in these areas during the visual-rotation condition and the curl-field condition is related to the higher torque requirements compared with the normal movement condition rather than to an error signal per se.

We performed a similar search for error-related voxels in the subcortical regions. The cerebellum (right lobule V and bilaterally in VIII) showed strongly increased activity during movements that experienced either kinematic or dynamic errors (Fig. 8*A*). Again, there was a remarkable degree of overlap between these regions. There was only one small region on the border of right lobule V and VI that showed higher activation in the visual-rotation than in the curl-field condition (MNI, 26, −46, −32; $p = 0.006$). No other subcortical sites were found that showed a significant difference between these two conditions.

We also conducted an anatomical ROI analysis for subcortical regions (Fig. 8*B*) (see above, Experiment 1: target errors versus execution errors). First, we replicated our result that the visual-rotation condition suppressed activity in the putamen compared with normal movement. This effect was significant in the right putamen ($t_{(15)} = -2.16$; $p = 0.047$) but not in the left putamen ($t_{(15)} = -1.22$; $p = 0.24$). The suppression of activity during movement error is even more remarkable, considering that the movements in the normal condition were considerably shorter in length and duration than in the error conditions (Table 1).

In contrast, the cerebellar cortex showed increased activity with any type of error, both for kinematic or dynamic (all $t > 4.07$; all $p < 0.004$). In contrast to primary motor cortex, the resistive field condition did not lead to increased activity in the cerebellum, indicating that the signal increase in the error conditions was not related to the higher torque requirements of the corrective movements.

In summary, we found that the structures involved in the correction of errors attributable to misestimation of dynamics (curl-field condition) were generally a subset of the neural areas involved in correction of movement errors attributable to misestimation of kinematics (visual-rotation condition). The overlapping areas involved the motor cortex, SII, an area along the postcentral sulcus, area 5, and the cerebellum lobules V and VIII. Motor cortex and SII were also highly activated by the resistive-field condition, which led to a similar torque output as the curl-field condition but did not demand error correction. In contrast, none of the ROIs in the basal ganglia were significantly activated by kinematic or dynamic errors. Only target errors, as shown in experiment 1, produced increased activity in the striatum.

Discussion

We compared the neural response with different types of reach errors: target errors (induced by target displacements), kinematic errors (induced by novel visual feedback), and dynamic errors (induced by the application of force fields). The motor system showed trial-to-trial adaptation in response to random execution errors but not random target errors.

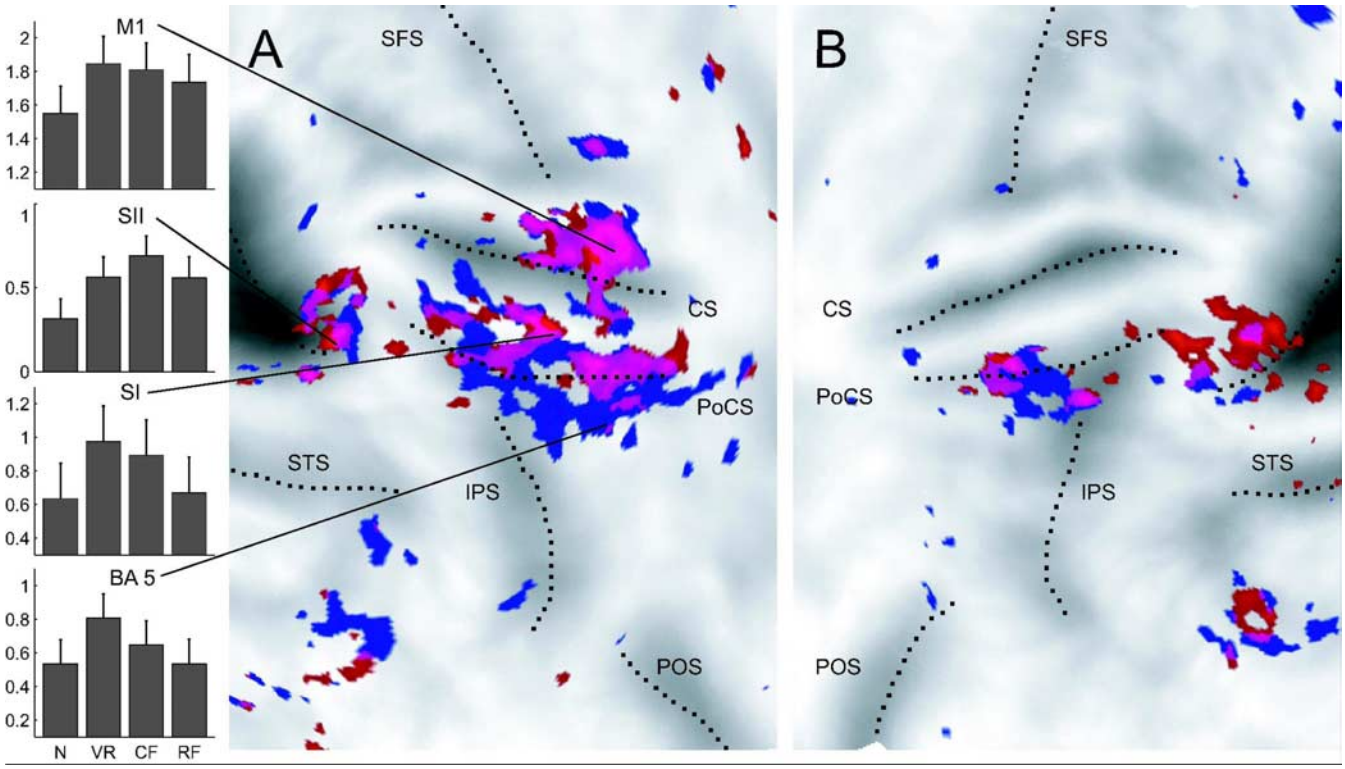

Figure 7. Activation in experiment 2 in the visual-rotation (blue) and curl-field (red) conditions relative to normal movements at a threshold of $t_{(16)} > 4$ for the left (***A***) and right (***B***) hemisphere is shown. Purple areas indicate overlap. The bar graphs show average percentage signal change in selected areas of the left hemisphere for normal (N), visual-rotation (VR), curl-field (CF), and resistive-field (RF) conditions. Abbreviations as in Figure 3

Target errors and goal change

Target errors, but not execution errors, activated the posterior SPL and the striatum. More lateral posterior parietal regions (e.g., IPSp) overlapped spatially with area "retIPS," implicated in a gaze-centered representation of reach targets (Medendorp et al., 2003, 2005). Recently, medial regions (e.g., SPLmed and POS) have been found to be more active during planning of reaching than during planning of saccades (Astafiev et al., 2003; Connolly et al., 2003), suggesting that these areas represent the current target for reaching movements. Given this functional role, the posterior SPL including the parieto-occipital sulcus constitutes a possible human homolog of the parietal-reach region (Snyder et al., 1998, 2000a,b; Battaglia-Mayer et al., 2000). Congruent with this hypothesis, we found that these areas showed increased activity when the target was updated during the reach.

In a classic positron emission tomography (PET) study, Desmurget et al. (2001) used a contrast similar to Equation 5 to identify regions involved in correction of reaching errors. They found an intraparietal site (approximately MNI −41, −48, 61) located anterior to the areas that we found active during target errors. It is possible that the errors in the PET study behaved like execution errors because the target displacements occurred during the saccade and therefore went unnoticed attributable to saccadic suppression. This hypothesis predicts that, unlike the target errors that we studied, target jumps that occur during a saccade would result in trial-to-trial adaptation.

We observed involvement of the striatum in the correction for target errors but not execution errors. This result is consistent with impaired on-line correction in Parkinson's disease when reach target jumped during the reach (Desmurget et al., 2004). Evidence for the role of the basal ganglia in on-line correction was also found in Huntington's disease patients, which demonstrated an inability to correct for large, externally imposed force pulses to the hand (Smith et al., 2000). Although it is not clear whether to categorize such external perturbations as goal or execution errors, it is possible that the observed deficits arose from an inability to maintain the behavioral goal throughout the movement.

We propose that reach goals are represented in the parietal reach region (Snyder et al., 2000b) and have to be rapidly switched when a target jump is detected. Recent evidence suggests the involvement of the striatum in this switching process (Zink et al., 2003; Cools et al., 2004). The selection and switching of the task-relevant goals may be achieved by the winner-take-all property of the cortical–striatal–cortical loop (Redgrave et al., 1999). Multiple possible target representations activate parallel subsets of striatal neurons, and inhibitory interconnections lead to disinhibition of only the strongest of these inputs (Jiang et al., 2003). Our finding that activity increases during target jumps, but decreases during visual rotation, suggests that the role of the putamen is limited to changes in the reach goal, without extending to on-line error correction in general.

No response to errors was found in the anterior cingulate, an area that has been connected to error detection and correction (Carter et al., 1998). We believe that errors that activate the cingulate are errors occurring when choosing a response under uncertainty (choice errors). In our study, there was never a choice; rather, errors arose during the execution of a (correctly) chosen action.

Execution errors and adaptation

We found that execution errors produced strong adaptive responses that specifically activated anterior aspects of the parietal cortex. Because we applied random perturbations to the arm, adaptation could never accumulate, leaving the participants in a

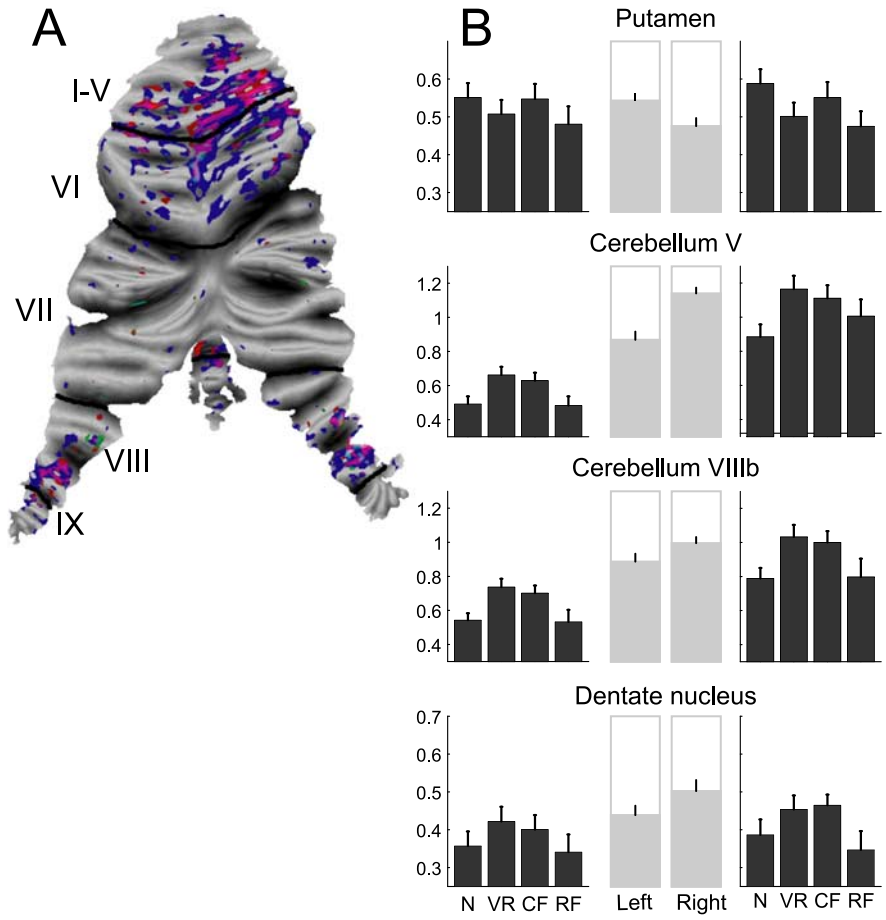

Figure 8. ***A***, Activation in experiment 2 in the visual-rotation (blue) and curl-field (red) conditions relative to normal movements at a threshold of $t_{(16)} > 4$ displayed on a surface representation of the cerebellum (Van Essen, 2002). ***B***, Percentage signal change (dark bars) in subcortical ROIs during normal (N), visual-rotation (VR), curl-field (CF), and resistive field (RF) conditions. The middle gray bars show the proportion of each ROI that was identified as movement related (average movement > rest; $p < 0.05$ uncorrected).

constant state of early learning. Nonetheless, we found that execution errors led to adaptation on the next trial, whereas hardly any adaptation occurred in response to target errors. This new method is advantageous in investigating learning because we can match the characteristics of errors and movements while dissociating the adaptation produced by these errors.

In previous adaptation studies (Clower et al., 1996; Inoue et al., 1997, 2000; Krakauer et al., 2004; Graydon et al., 2005), it was less clear whether increases in neural activity during early learning were caused by error-driven adaptive processes or by changes in movements kinematics. Conversely, because learning did not accumulate in our study, our results do not speak to the question of whether neural representation shifts as a new internal model is formed (Shadmehr and Holcomb, 1997; Imamizu et al., 2000; Nezafat et al., 2001; Krakauer et al., 2004). Despite this limitation, our result shows that regions bilaterally along the postcentral sulcus and in area 5 receive execution error signals, making them candidates for areas that perform and learn new visuomotor transformations.

Although these conclusions are consistent with some findings (Inoue et al., 1997, 2000; Imamizu et al., 2004), they contradict other studies reporting involvement of posterior parietal regions in the acquisition of visuomotor transformations (Clower et al., 1996; Grefkes et al., 2004; Graydon et al., 2005). The involvement of the posterior SPL in these studies may be explained by additional eye movements or replanning of the movement (Graydon et al., 2005) or the need to attend to a target object (Grefkes et al., 2004).

Previous work in the nonhuman primate has also suggested the involvement of dorsal premotor cortex (Wise et al., 1998) and supplementary motor area (SMA) (Padoa-Schioppa et al., 2004) in visuomotor adaptation. In experiment 2, we found that the dorsal premotor cortex significantly responded to kinematic errors. In experiment 1, this region also showed slightly higher responses to kinematic than to target errors, although this result was not significant on a clusterwise level. In the SMA, however, we found no consistent response to errors.

The role of the cerebellum and motor cortex in error correction and adaptation

Cerebellar lesions profoundly reduce the ability to adapt to both dynamic and kinematic errors (Martin et al., 1996; Baizer et al., 1999; Maschke et al., 2004; Diedrichsen et al., 2005; Smith and Shadmehr, 2005). In contrast, on-line corrections to large perturbations are partly preserved (Smith et al., 2000). Therefore, we expected increased activity in the cerebellar cortex in response to execution errors but not to target errors. This hypothesis is reasonable given that climbing fibers are thought to carry error signals that cause adaptation (Kitazawa et al., 1998), and climbing fiber activity contributes substantially to the metabolic signal from the cerebellar cortex (Zhang et al., 2003).

All task-related areas in the cerebellum (lobules V, VI, and VIII and dentate) showed strongly increased activity to both execution and target errors. No area was selectively activated by execution errors. It is unclear how to resolve the contradiction between patient and functional imaging results. Given the fractured somatotopy of the cerebellum (Shambes et al., 1978), it is possible that we failed to detect small regions specific to execution errors. Based on the current limitations in spatial resolution, however, we have to conclude that the cerebellar BOLD signal is driven equivalently by target and execution errors. This finding is consistent with the observation of increases in cerebellar activity during early learning phases attributable to execution errors (Imamizu et al., 2000), as well as when the need for feedback control is increased (Seidler et al., 2004). Whether this activity only reflects on-line error correction, or possibly also adaptive processes, is still a matter of debate (Seidler et al., 2002).

We also failed to detect a differential role for the motor cortex in execution versus target errors. This is surprising because adaptation to force fields (Gandolfo et al., 2000; Li et al., 2001) or visual rotations (Paz et al., 2003) lead to lasting changes in response properties of primary motor cortex cells. It is possible that these changes would become apparent when adaptation is allowed to accumulate.

Comparisons of kinematic and dynamic errors

Neural responses specific to dynamic and kinematic errors were found in primarily overlapping areas along the postcentral sulcus. Only area 5 and the cerebellum on the border between lobules V and VI were more activated by kinematic than by dynamic errors. Thus, our results provide evidence that kinematic and dynamic transformations are performed in a continuous cascade ranging from area 5, in which very little force-related activity is found (Kalaska et al., 1990), forward into sensory motor cortex.

These transformations may be performed in an overlapping manner, most likely by populations of neurons that exhibit multiplicative tuning with respect to visual properties of hand and target positions, proprioceptive arm position, and dynamics (Hwang et al., 2003). Congruent with this hypothesis is the observation that dynamic and kinematic adaptation processes can interfere with each other (Tong et al., 2002). Based on our results, it appears that kinematic and dynamic transformations are not performed in two anatomically separate areas but rather in one continuous, overlapping cascade.

References

Ashburner J, Friston KJ (1999) Nonlinear spatial normalization using basis functions. Hum Brain Mapp 7:254–266.

Astafiev SV, Shulman GL, Stanley CM, Snyder AZ, Van Essen DC, Corbetta M (2003) Functional organization of human intraparietal and frontal cortex for attending, looking, and pointing. J Neurosci 23:4689–4699.

Atkeson CG (1989) Learning arm kinematics and dynamics. Annu Rev Neurosci 12:157–183.

Baizer JS, Kralj-Hans I, Glickstein M (1999) Cerebellar lesions and prism adaptation in macaque monkeys. J Neurophysiol 81:1960–1965.

Battaglia-Mayer A, Ferraina S, Mitsuda T, Marconi B, Genovesio A, Onorati P, Lacquaniti F, Caminiti R (2000) Early coding of reaching in the parietooccipital cortex. J Neurophysiol 83:2374–2391.

Carter CS, Braver TS, Barch DM, Botvinick MM, Noll D, Cohen JD (1998) Anterior cingulate cortex, error detection, and the online monitoring of performance. Science 280:747–749.

Clower DM, Hoffman JM, Votaw JR, Faber TL, Woods RP, Alexander GE (1996) Role of posterior parietal cortex in the recalibration of visually guided reaching. Nature 383:618–621.

Connolly JD, Andersen RA, Goodale MA (2003) FMRI evidence for a "parietal reach region" in the human brain. Exp Brain Res 153:140–145.

Cools R, Clark L, Robbins TW (2004) Differential responses in human striatum and prefrontal cortex to changes in object and rule relevance. J Neurosci 24:1129–1135.

Corbetta M, Akbudak E, Conturo TE, Snyder AZ, Ollinger JM, Drury HA, Linenweber MR, Petersen SE, Raichle ME, Van Essen DC, Shulman GL (1998) A common network of functional areas for attention and eye movements. Neuron 21:761–773.

Curtis CE, Cole MW, Rao VY, D'Esposito M (2005) Canceling planned action: an fMRI study of countermanding saccades. Cereb Cortex 15:1281–1289.

Desmurget M, Grafton S (2000) Forward modeling allows feedback control for fast reaching movements. Trends Cogn Sci 4:423–431.

Desmurget M, Epstein CM, Turner RS, Prablanc C, Alexander GE, Grafton ST (1999) Role of the posterior parietal cortex in updating reaching movements to a visual target. Nat Neurosci 2:563–567.

Desmurget M, Grea H, Grethe JS, Prablanc C, Alexander GE, Grafton ST (2001) Functional anatomy of nonvisual feedback loops during reaching: a positron emission tomography study. J Neurosci 21:2919–2928.

Desmurget M, Gaveau V, Vindras P, Turner RS, Broussolle E, Thobois S (2004) On-line motor control in patients with Parkinson's disease. Brain 127:1755–1773.

Diedrichsen J (2005) Surface statistics using Caret. Available online at: www.bme.jhu.edu/~jdiedric/imaging/surfacestats.htm.

Diedrichsen J, Shadmehr R (2005) Detecting and adjusting for artifacts in fMRI time series data. NeuroImage 27:624–634.

Diedrichsen J, Verstynen T, Lehman SL, Ivry RB (2005) Cerebellar involvement in anticipating the consequences of self-produced actions during bimanual movements. J Neurophysiol 93:801–812.

Donchin O, Francis JT, Shadmehr R (2003) Quantifying generalization from trial-by-trial behavior of adaptive systems that learn with basis functions: theory and experiments in human motor control. J Neurosci 23:9032–9045.

Flash T, Sejnowski TJ (2001) Computational approaches to motor control. Curr Opin Neurobiol 11:655–662.

Friston K, Holmes AP, Ashburner J (1999) Statistical Parameter Mapping (SPM). Available at www.fil.ion.ucl.ac.uk/spm.

Friston KJ, Worsley KJ, Frackowiak RSJ, Mazziotta JC, Evans AC (1994) Assessing the significance of focal activations using their spatial extent. Hum Brain Mapp 1:214–220.

Gandolfo F, Li C, Benda BJ, Schioppa CP, Bizzi E (2000) Cortical correlates of learning in monkeys adapting to a new dynamical environment. Proc Natl Acad Sci USA 97:2259–2263.

Graydon FX, Friston KJ, Thomas CG, Brooks VB, Menon RS (2005) Learning-related fMRI activation associated with a rotational visuomotor transformation. Brain Res Cogn Brain Res 22:373–383.

Grefkes C, Geyer S, Schormann T, Roland P, Zilles K (2001) Human somatosensory area 2: observer-independent cytoarchitectonic mapping, interindividual variability, and population map. NeuroImage 14:617–631.

Grefkes C, Ritzl A, Zilles K, Fink GR (2004) Human medial intraparietal cortex subserves visuomotor coordinate transformation. NeuroImage 23:1494–1506.

Hwang EJ, Donchin O, Smith MA, Shadmehr R (2003) A gain-field encoding of limb position and velocity in the internal model of arm dynamics. PLoS Biol 1:E25.

Imamizu H, Miyauchi S, Tamada T, Sasaki Y, Takino R, Puetz B, Yoshioka T, Kawato M (2000) Human cerebellar activity reflecting an acquired internal model of a new tool. Nature 403:192–195.

Imamizu H, Kuroda T, Yoshioka T, Kawato M (2004) Functional magnetic resonance imaging examination of two modular architectures for switching multiple internal models. J Neurosci 24:1173–1181.

Inoue K, Kawashima R, Satoh K, Kinomura S, Goto R, Sugiura M, Ito M, Fukuda H (1997) Activity in the parietal area during visuomotor learning with optical rotation. NeuroReport 8:3979–3983.

Inoue K, Kawashima R, Satoh K, Kinomura S, Sugiura M, Goto R, Ito M, Fukuda H (2000) A PET study of visuomotor learning under optical rotation. NeuroImage 11:505–516.

Jiang H, Stein BE, McHaffie JG (2003) Opposing basal ganglia processes shape midbrain visuomotor activity bilaterally. Nature 423:982–986.

Kalaska JF, Cohen DA, Prud'homme M, Hyde ML (1990) Parietal area 5 neuronal activity encodes movement kinematics, not movement dynamics. Exp Brain Res 80:351–364.

Kelly RM, Strick PL (2003) Cerebellar loops with motor cortex and prefrontal cortex of a nonhuman primate. J Neurosci 23:8432–8444.

Kitazawa S, Kimura T, Yin PB (1998) Cerebellar complex spikes encode both destinations and errors in arm movements. Nature 392:494–497.

Koyama M, Hasegawa I, Osada T, Adachi Y, Nakahara K, Miyashita Y (2004) Functional magnetic resonance imaging of macaque monkeys performing visually guided saccade tasks: comparison of cortical eye fields with humans. Neuron 41:795–807.

Krakauer JW, Ghilardi MF, Ghez C (1999) Independent learning of internal models for kinematic and dynamic control of reaching. Nat Neurosci 2:1026–1031.

Krakauer JW, Ghilardi MF, Mentis M, Barnes A, Veytsman M, Eidelberg D, Ghez C (2004) Differential cortical and subcortical activations in learning rotations and gains for reaching: a PET study. J Neurophysiol 91:924–933.

Li CS, Padoa-Schioppa C, Bizzi E (2001) Neuronal correlates of motor performance and motor learning in the primary motor cortex of monkeys adapting to an external force field. Neuron 30:593–607.

Logothetis NK (2003) The underpinnings of the BOLD functional magnetic resonance imaging signal. J Neurosci 23:3963–3971.

Martin TA, Keating JG, Goodkin HP, Bastian AJ, Thach WT (1996) Throwing while looking through prisms. I. Focal olivocerebellar lesions impair adaptation. Brain 119:1183–1198.

Maschke M, Gomez CM, Ebner TJ, Konczak J (2004) Hereditary cerebellar ataxia progressively impairs force adaptation during goal-directed arm movements. J Neurophysiol 91:230–238.

Mattar AA, Gribble PL (2005) Motor learning by observing. Neuron 46:153–160.

Medendorp WP, Goltz HC, Vilis T, Crawford JD (2003) Gaze-centered updating of visual space in human parietal cortex. J Neurosci 23:6209–6214.
Medendorp WP, Goltz HC, Crawford JD, Vilis T (2005) Integration of target and effector information in human posterior parietal cortex for the planning of action. J Neurophysiol 93:954–962.
Neggers SF, Bekkering H (2001) Gaze anchoring to a pointing target is present during the entire pointing movement and is driven by a nonvisual signal. J Neurophysiol 86:961–970.
Nezafat R, Shadmehr R, Holcomb HH (2001) Long-term adaptation to dynamics of reaching movements: a PET study. Exp Brain Res 140:66–76.
Padoa-Schioppa C, Li CS, Bizzi E (2004) Neuronal activity in the supplementary motor area of monkeys adapting to a new dynamic environment. J Neurophysiol 91:449–473.
Paz R, Boraud T, Natan C, Bergman H, Vaadia E (2003) Preparatory activity in motor cortex reflects learning of local visuomotor skills. Nat Neurosci 6:882–890.
Pruessmann KP, Weiger M, Scheidegger MB, Boesiger P (1999) SENSE: sensitivity encoding for fast MRI. Magn Reson Med 42:952–962.
Redgrave P, Prescott TJ, Gurney K (1999) The basal ganglia: a vertebrate solution to the selection problem? Neuroscience 89:1009–1023.
Schluppeck D, Glimcher PW, Heeger DJ (2005) Topographic organization for delayed saccades in human posterior parietal cortex. J Neurophysiol 94:1372–1384.
Schmahmann JD, Doyon J, Toga A, Petrides M, Evans A (2000) MRI atlas of the human cerebellum. San Diego: Academic.
Seidler RD, Purushotham A, Kim SG, Ugurbil K, Willingham D, Ashe J (2002) Cerebellum activation associated with performance change but not motor learning. Science 296:2043–2046.
Seidler RD, Noll DC, Thiers G (2004) Feedforward and feedback processes in motor control. NeuroImage 22:1775–1783.
Sereno MI, Pitzalis S, Martinez A (2001) Mapping of contralateral space in retinotopic coordinates by a parietal cortical area in humans. Science 294:1350–1354.
Shadmehr R, Holcomb HH (1997) Neural correlates of motor memory consolidation. Science 277:821–825.
Shadmehr R, Mussa-Ivaldi FA (1994) Adaptive representation of dynamics during learning of a motor task. J Neurosci 14:3208–3224.
Shadmehr R, Wise R (2004) Motor learning and memory for reaching and pointing. In: The cognitive neurosciences, Ed 3 (Gazzaniga MS, ed), pp 511–524. Boston: MIT.
Shambes GM, Gibson JM, Welker W (1978) Fractured somatotopy in granule cell tactile areas of rat cerebellar hemispheres revealed by micromapping. Brain Behav Evol 15:94–140.
Smith MA, Shadmehr R (2005) Intact ability to learn internal models of arm dynamics in Huntington's disease but not cerebellar degeneration. J Neurophysiol 93:2809–2821.
Smith MA, Brandt J, Shadmehr R (2000) Motor disorder in Huntington's disease begins as a dysfunction in error feedback control. Nature 403:544–549.
Snyder LH, Batista AP, Andersen RA (1998) Change in motor plan, without a change in the spatial locus of attention, modulates activity in posterior parietal cortex. J Neurophysiol 79:2814–2819.
Snyder LH, Batista AP, Andersen RA (2000a) Saccade-related activity in the parietal reach region. J Neurophysiol 83:1099–1102.
Snyder LH, Batista AP, Andersen RA (2000b) Intention-related activity in the posterior parietal cortex: a review. Vision Res 40:1433–1441.
Sunaert S, Van Hecke P, Marchal G, Orban GA (1999) Motion-responsive regions of the human brain. Exp Brain Res 127:355–370.
Thoroughman KA, Shadmehr R (2000) Learning of action through adaptive combination of motor primitives. Nature 407:742–747.
Tong C, Wolpert DM, Flanagan JR (2002) Kinematics and dynamics are not represented independently in motor working memory: evidence from an interference study. J Neurosci 22:1108–1113.
Tootell RB, Hadjikhani N, Hall EK, Marrett S, Vanduffel W, Vaughan JT, Dale AM (1998) The retinotopy of visual spatial attention. Neuron 21:1409–1422.
Van Essen DC (2002) Surface-based atlases of cerebellar cortex in the human, macaque, and mouse. Ann NY Acad Sci 978:468–479.
Van Essen DC (2005) A population-average, landmark- and surface-based (PALS) atlas of the human cerebral cortex. NeuroImage, in press.
Van Essen DC, Dickson J, Harwell J, Hanlon D, Anderson CH, Drury HA (2001) An integrated software system for surface-based analyses of cerebral cortex. J Am Med Inform Assoc 41:1359–1378.
Wainscott SK, Donchin O, Shadmehr R (2005) Internal models and contextual cues: encoding serial order and direction of movement. J Neurophysiol 93:786–800.
Wise SP, Moody SL, Blomstrom KJ, Mitz AR (1998) Changes in motor cortical activity during visuomotor adaptation. Exp Brain Res 121:285–299.
Worsley KJ, Marrett S, Neelin P, Vandal AC, Friston KJ, Evans AC (1996) A unified statistical approach for determining significant voxels in images of cerebral activation. Hum Brain Mapp 12:900–918.
Zhang Y, Forster C, Milner TA, Iadecola C (2003) Attenuation of activity-induced increases in cerebellar blood flow by lesion of the inferior olive. Am J Physiol Heart Circ Physiol 285:H1177–H1182.
Zink CF, Pagnoni G, Martin ME, Dhamala M, Berns GS (2003) Human striatal response to salient nonrewarding stimuli. J Neurosci 23:8092–8097.